Journal of Colloid and Interface Science 514 (2018) 433–442

Contents lists available at ScienceDirect

Journal of Colloid and Interface Science

journal homepage: www.elsevier.com/locate/jcis

Regular Article

Chitosan-fatty acid interaction mediated growth of Langmuir monolayer and Langmuir-Blodgett films

Ikbal Ahmed [a], Lucky Dildar [a], Anamul Haque [a], Prasun Patra [a], Mala Mukhopadhyay [b,1], Satyajit Hazra [b], Manish Kulkarni [c], Sabu Thomas [d], Jasper R. Plaisier [e], Shyamal Baran Dutta [f], Jayanta Kumar Bal [a,f,*]

[a] Centre for Research in Nanoscience and Nanotechnology, University of Calcutta, Technology Campus, Block JD2, Sector III, Saltlake City, Kolkata 700098, India
[b] Saha Institute of Nuclear Physics, 1/AF Bidhannagar, Kolkata 700064, India
[c] Center for Nanosciences, Indian Institute of Technology, Kanpur 208016, India
[d] International and Inter University Centre for Nanoscience and Nanotechnology, Mahatma Gandhi University, Kottayam 686560, India
[e] Elettra - Sincrotrone Trieste S.C.p.A., S.S. 14 km 163.5 in Area Science Park, 34149 Basovizza, Trieste, Italy
[f] Abhedananda Mahavidyalaya, University of Burdwan, Sainthia 731234, India

HIGHLIGHTS

- Chitosan-fatty acid interactions at air–water interface.
- Interactions modification by chitosan mole fraction and temperature.
- Relocation of chitosan on solid substrate employing Langmuir-Blodgett technique via mixing with fatty acid.
- Surface pressure induced 2D to 3D structural transition of chitosan-fatty LB films.

GRAPHICAL ABSTRACT

We have demonstrated that chitosan has strong affinity with fatty acid (stearic acid) and adsorbs at the fatty acid monolayer at air–water interface, despite its lack of surface activity. Chitosan insertion caused an expansion of chitosan-fatty acid mixed monolayers and reduced the elasticity and made the film heterogeneous. Chitosan endorses a local distortion of the fatty acid tails involving electrostatic, dipolar and hydrophobic interactions. The results could be rationalized in terms of a model in which at low surface pressure chitosan is situated at interface, interacting with stearic acid molecules via electrostatic and hydrophobic interactions whereas at high pressure chitosan mainly located at subsurface beneath stearic acid molecules. In the latter case the interaction is predominantly electrostatic yielding very small contribution to the surface pressure. Reduction of temperature allows more number of chitosan molecules to reach surface. In addition, chitosan could be transferred onto solid supports employing LB technique by mixing with fatty acid.

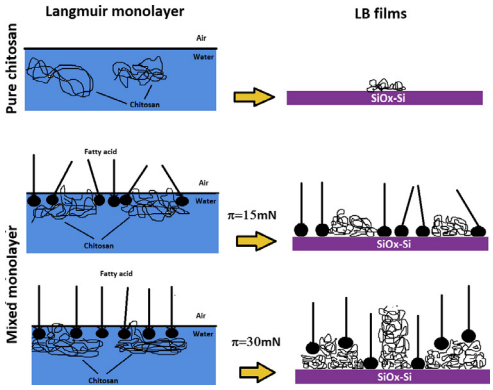

ARTICLE INFO

Article history:
Received 19 September 2017
Revised 13 December 2017

ABSTRACT

The interaction of chitosan with bio-membranes, which plays important role in deciding its use in biological applications, is realized by investigating the interaction of chitosan with stearic acid (fatty acid) in Langmuir monolayers (at air–water interface) and Langmuir-Blodgett (LB) films (after transferring it onto

* Corresponding author at: Abhedananda Mahavidyalaya, University of Burdwan, Sainthia 731234, India.
E-mail address: jayanta.bal@gmail.com (J.K. Bal).
[1] Present address: B R A Bihar University, Muzaffarpur 842001, India.

https://doi.org/10.1016/j.jcis.2017.12.037

Accepted 14 December 2017
Available online 15 December 2017

Keywords:
Chitosan
Fatty acid
Langmuir monolayer
Langmuir-Blodgett film
Isotherm
Compressibility
Elasticity
Gibb's free energy

solid substrate). It is found from the pressure-area isotherms that the chitosan insertion causes an expansion of chitosan-fatty acid hybrid monolayers, which reduces the elasticity and make the film heterogeneous. It is likely that at low surface pressure chitosan is situated at the interface, interacting with stearic acid molecules via electrostatic and hydrophobic interactions whereas at high pressure chitosan mainly located at subsurface beneath stearic acid molecules. In the latter case the interaction is predominantly electrostatic yielding very small contribution to the surface pressure. The reduction of temperature of the subphase water allows more number of chitosan molecules to reach surface to increase the pressure/interaction. On the other hand, although pure chitosan is found difficult to relocate on the substrate from air-water interface due to its hydrophilic-like nature, it alongside stearic acid (amphiphilic molecules) can be transferred onto substrate using LB technique as evident from infrared spectra. Their out-of-plane and in-plane structures, as extracted from two complementary surface sensitive techniques- X-ray reflectivity and atomic force microscopy, are found strongly dependent on the chitosan mole fraction and the deposition pressure. These analysis of the film-structure will essentially allow one to model the system better and provide better insight into the interaction.

1. Introduction

Chitosan (CHS), being a polysaccharide of rich physicochemical properties, has attracted a great deal of research worldwide. It is widely used in medicine [1,2], food preservation [3], cosmetics [4,5], antibacterial agent [3] and biotechnology [6] owing to its biocompatibility, biodegradability and polycationic nature. In most of these applications CHS has to interact with bio-membrane surfaces. Being biocompatible means that CHS can interact with biomolecules without degrading them. This unique characteristic brings CHS into spotlight as a green polymer. CHS is normally prepared by alkaline deacetylation of chitin, which is extracted from the skeletal structures of crustaceans, insects, mushrooms and cell of fungi. Its cationic nature leads to a strong interaction with negatively charged entities, including many fatty acids, lipids and proteins. Fäldt et al. [7] investigated the interaction between CHS and emulsified lipids. They reported that CHS shields negatively charged lipid particles in the intestine and this process is likely to influence the restoration of lipids in the intestinal tract. CHS is being considered in various countries as a dietary supplement of human consumption [8,9]. However, concern has arisen about the fact that certain promotional campaigns advertise CHS as a fat-binding active agent towards all kinds of lipids with no supporting scientific proof. Magdassi et al. [10] studied the interactions between CHS and lecithin. Sathirakul et al. [11] and Muzzarelli et al. [12] compared the lipid binding capacity of CHS. The hydrophilicity, high viscosity, and insolubility of CHS inhibit in proper utilization. This was overcame by making a conjugate with biocompatible fatty acids (e.g. stearic acid) [13]. Therefore, understanding the interactions involved in the process of binding CHS with stearic acid (SA) is of paramount interest. But still the mechanism of these interactions is not well understood.

One possible way to investigate this interaction, in molecular-level, is to study the interaction of CHS with lipids or fatty acids, such as SA in the form of Langmuir monolayers, which can serve as simplified model for the cell membrane [14,15]. A Langmuir film is formed at air-water interfaces when amphiphilic, insoluble (in water) molecules are spread over the LB trough through a solution of volatile solvents [16]. After evaporation, the hydrophobic parts of the amphiphilic molecules are directed toward the air, whereas the hydrophilic ones are anchored to the aqueous subphase. The compression of molecules at the air-water interface enables to increase their density and packing, leading to changes in surface tension. In addition, deposited monolayer film can be studied as reliable model for lipid stacking in cell membrane structures and can be applied in biosensor devices.

The bulk properties of CHS in solution are well-known [17–20] but its surface properties at air-water interface are rarely studied [21–23]. It was clear that CHS is not surface active at bare water surface, but becomes surface active in presence of lipids and fatty acids [24–26]. However, there is still a lack of understanding about the surface orientation of CHS in presence of lipids and fatty acids, the residence of CHS at the air-water interface, the interaction involved. Though a numerous literature exploring viscoelastic properties (e.g. elasticity or compressibility) of CHS-lipids and CHS-fatty acids hybrid systems are present [21–23,25], but their thermodynamic (excess Gibb's free energy of mixing) and thermal (temperature dependent) properties remain unexplored. On the other hand, a model of CHS containing phospholipid film was drawn [23] on the basis of nanogravimetry measurements, where the transferred amount (nanogram) was calculated at each stroke with QCM. This corresponds to the adsorbed amount and not the structure of deposited films. The structure of LB films containing CHS is less reported. In this paper we reported the interactions of CHS with SA at the air-water interface by analysing the pressure-area (π-A) isotherms. This study is performed with particular emphasis on how CHS can modify the packing and ordering of the Langmuir monolayer and the transferred LB films. The structure of hybrid Langmuir monolayer is confirmed by measuring the structure of LB films using two complementary techniques, such as X-ray reflectivity (XRR) and atomic force microscopy (AFM).

2. Materials and methods

2.1. Materials and chemicals

SA and CHS (molecular weight 1526.4 g/mole, 75–80% deaceylated) were purchased from Sigma Aldrich Co. and Sisco Research Laboratories Pvt. Ltd., respectively and they were used as received. Solutions of pure CHS having concentration of 6.25, 12.5 and 50 mM were prepared in chloroform (mixed with 1% acetic acid in volume). SA solution of 50 mM was prepared using chloroform solvent. This SA solution was mixed with three different concentrated CHS solutions (taking same volume of both) yielding the concentration ratios 1:1, 1:4 and 1:8.

2.2. Substrate cleaning

For the preparation of films Si(1 0 0) substrates were cleaned by RCA-treatment (Radio Corporation of America). The details of RCA cleaning were described elsewhere [27]. In RCA cleaning, the Si surfaces (of size $\approx 25 \times 15$ mm^2) were made hydrophilic by introducing hydroxyl group (–OH) after boiling them in a mixture of ammonium hydroxide (NH_4OH, Sigma-Aldrich, 25%), hydrogen peroxide (H_2O_2, Acros Organics, 39%), and Milli-Q water (H_2O:NH_4OH:H_2O_2=2:1:1, by volume) for 10 min at 100 °C. Then

the substrates were washed in Milli-Q water and dried prior before film deposition.

2.3. Preparation of films at air-water interface and on substrate

Langmuir monolayers and LB films were fabricated with a LB trough (Apex Instruments, model No.: LBXD-NT) of inner working area: 560 mm (*length*) × 200 mm (*width*) × 5 mm (*height*), kept in a clean environment. The LB trough was made of PTTE trough with two barriers moving towards each other. In middle of the trough a Wilhelmy plate (a filter paper having a dimension of 10 × 25 mm^2) was dipped into the aqueous phase to measure the change in surface tension manifested as surface pressure. The LB trough was thoroughly cleaned with water purified with a Milli-Q system (Resistivity ~ 18 MΩ cm) and then with ethanol followed by purified water for making the trough absolutely dust free. For mixed monolayer study, same volume of SA solution was mixed with same volume of different concentrated CHS solutions before spreading. These homogeneously mixed solutions were spread drop-by-drop all over the trough between two movable surface barriers using a Hamilton syringe (precision of 2.5 μL). The solvent was allowed to evaporate for 10 to 15 min until the pressure stabilizes and then the monolayer was compressed to get surface pressure (mN/m) vs area per molecule (nm^2) ($\pi - A$) isotherm (at a fixed temperature of 22 °C). All the isotherms were recorded in a constant compression speed of 10 mm/min. The isotherm was recorded until it collapses at a certain pressure, known as collapse pressure (π_c). The temperature of the subphase water had decreased down to 8 °C from room temperature using a chiller (First Source Company). LB films were deposited at two constant pressures π = 30 mN/m and 15 mN/m onto RCA cleaned Si(1 0 0) substrates in a single upstroke which rendered a transfer ratio closed to 0.9. All the films were deposited maintaining a constant barrier compression speed and expansion speed of 8 mm/min. The lifting and dipping speed of substrates for LB deposition was maintained at 5 mm/min. After deposition, the films were kept for 10 min above the subphase for drying before collecting them.

2.4. Characterization

2.4.1. X-ray reflectivity and infrared spectroscopy

XRR measurements were carried out at the MCX beamline [28] of Elettra - Sincrotrone Trieste. The wavelength used was 1.54 Å. The beamline is equipped with a high resolution four-circle diffractometer and a three (X, Y, and Z) translational stage. Scattered intensities were recorded using a scintillator detector behind a set of receiving slits. Data were taken in specular condition, i.e., the incident angle is equal to the reflected angle and both are in a scattering plane. Under such condition, a non-vanishing wave vector component, q_z, is given by $(4\pi/\lambda)\mathrm{Sin}\theta$ with resolution of 0.0010 $Å^{-1}$. We also verified the samples in our lab source (D8 Discover, Bruker AXS). XRR technique essentially provides an electron density profile (EDP), i.e., in-plane (x–y) average electron density (ρ) as a function of depth (z) in high resolution [29]. From EDP it is possible to estimate film thickness, electron density, and interfacial roughness [30,31]. Analysis of XRR data is carried out using the matrix technique [29]. In general, the electron-density variation in a specimen is determined by assuming a model and comparing the simulated profile with the experimental data. EDP is extracted from the fitting of experimental XRR data. For the analysis, each film is divided into a number of layers including roughness at each interface [29,32]. An instrumental resolution in the form of a Gaussian function and a constant background were also included at the time of data analysis. However elemental detection is not possible by XRR as it is only probing average electron density of the films. Hence there would be an uncertainty about the deposition of a particular species (e.g. CHS molecules) along with hybrid films (e.g. CHS-SA mixed films) on substrate. The presence of CHS in such hybrid LB films is inferred from transmission Fourier transform infrared spectroscopy (FTIR) measurements with a Jasco FT/IR-6300 spectrometer.

2.4.2. Atomic force microscopy

Surface morphology of the films were collected by an AFM (Agilent 5500 and Asylum Research) and scans were performed over several portions of the films for different scan areas after completion of XRR measurements. AFM images were collected in non-contact mode using silicon cantilever (dimensions: 125 μm × 30 μm, spring constant = 42 N/m, resonance frequency = 320 kHz) and sharp needle-like tip in ambient condition to minimize the tip-induced modification of sample surface respectively. Windows Scanning x Microscope (WSxM, where x is force, tunneling, near-optical, etc.) software [33] was used for image processing and analysis.

3. Results and discussion

3.1. Monolayer characteristics

3.1.1. Surface pressure-area isotherm of pure stearic acid and chitosan

Fig. 1 depicts surface pressure (π)-area (A) isotherm of pure CHS and pure SA. The monolayer of SA exhibits typical isotherm with a change of slope at π = 27 mN/m, where a transition from the liquid condensed to the solid state occurs. Similar values are reported by Seoane et al. [34] and Barraza et al.[25]. The extrapolated area (A_{ex}), calculated from the isotherm curve by extending the linear part to zero surface pressure axis, is found around 22 $Å^2$/molecule. The area of condensation threshold (A_0), where phase transition from gaseous to liquid occurs at $\pi_{G\text{-}L}$ = 0.9 mN/m, is obtained around 24 $Å^2$/molecule. Although the value of A_{ex} is in quite agreement to the reported value by Seoane et al. [34] and Barraza et al. [25], A_0 value differs appreciably.

We recorded the isotherm until the monolayer collapses. The collapse pressure (π_c) is reached after the solid phase, followed by a downward drift of surface pressure. The surface pressure starts falling because of multilayer formation. The study of collapse has received special attention because the mechanism that leads a two-dimensional (2D) structure to form a three-dimensional (3D) structure is not fully understood [35]. However, the collapse pressure of SA is found to be π_c = 60 mN/m. Although the same value was obtained by Wydro et al. [21], π_c may vary depending on the compression rate of monolayer. Probably due to this reason a lower value of π_c around 45 mN/m was observed by Barraza et al. [24]. On the other hand, no abrupt increase in surface pressure of pure CHS is encountered. Surface pressure does not alter appreciably when the barriers are compressed. Such lack of surface activity can be explained considering the solubility of CHS in water.

3.1.2. Surface pressure-area isotherm of CHS-SA mixed monolayer

The isotherms of CHS-SA hybrid monolayers with varying mole fraction of CHS are depicted in Fig. 2. They form stable monolayer with a well-defined phase transition from gaseous to liquid near $\pi_{G\text{-}L}$ = 1 mN/m and from liquid to solid phase around $\pi_{L\text{-}S}$ = 17–24 mN/m. The collapse pressures π_c are found to be 52, 44 and 39 mN/m for 1:8, 1:4 and 1:1 mixed monolayers, respectively. So a systematic decrease in π_c with higher concentration of CHS is evident. Such variations can be attributed to the movement of CHS from the bulk subphase to the interface. Hydrophobic interactions between the hydrocarbon tails of SA and CHS promote CHS to appear with SA monolayer and to occupy the empty spaces resulting in the expansion of the monolayer. Similar results were

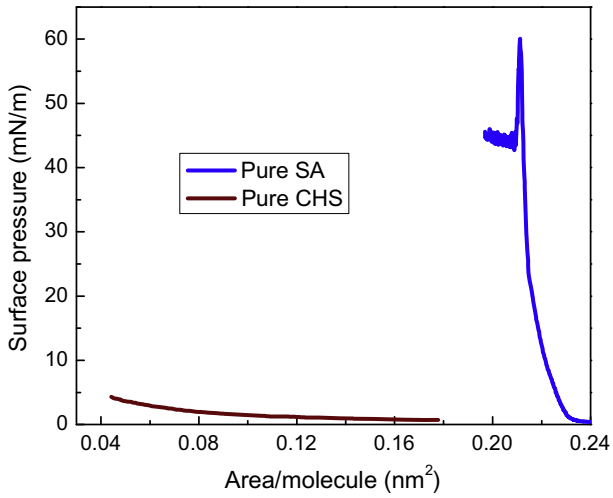

Fig. 1. Isotherm of pure chitosan (CHS) and pure stearic acid (SA).

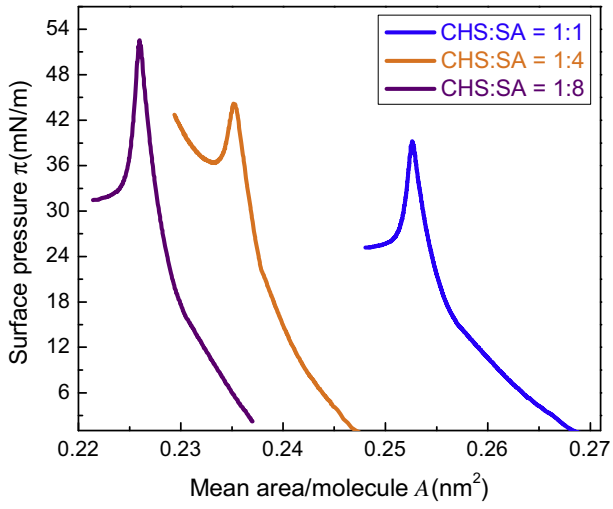

Fig. 2. Isotherm of mixed monolayer of chitosan (CHS) and stearic acid (SA).

obtained by Wydro et al. [21]. Such expansion endorses that CHS is competent enough to absorb onto a SA monolayer. CHS is not completely forced out to the bulk water rather it forms a subsurface interacting with SA polar heads (—COOH group). However, some of the CHS molecules might embedded within the SA monolayer matrix prior to participate in isotherm. On the other hand, Gargallo et al. [36] reported that the π_c of poly(maleicanhydride-alt-stearyl methacrylate) decreased from 52 to 31 mN/m with the addition of 3 g/L of CHS in the acetic acid solution (0.3 mol/L). In contrast, unsaturated acids (e.g. oleic, linoleic acids etc.) show reverse behavior. Perhaps the incorporation of CHS makes the SA monolayer flexible. This flexibility facilitates collapse to take place at lower pressure, which signifies that hybrid monolayer takes 3D structure from 2D more rapidly with increasing concentration of CHS. Such characteristics indicate a well-defined conjugation between CHS and SA in hybrid monolayer.

To look over the miscibility of the binary mixture and how individual components (e.g. CHS and SA) interact with each other in mixture, the excess area per molecule (A_{exc}) and the excess Gibb's free energy (ΔG_{exc}) are calculated. A_{exc} is estimated by the departure of experimentally determined area per molecule (A_{12}) from the ideal area per molecule (A_{id}) [37]:

$$A_{exc} = A_{12} - A_{id} \tag{1}$$

where $A_{id} = A_{SA}X_{SA} + A_{CHS}X_{CHS}$.

Here A_{SA} and A_{CHS} are the mean molecular areas of SA and CHS, respectively. X_{SA} and X_{CHS} are their corresponding mole fraction. The excess area A_{exc} is found more prominent for X_{CHS} = 0.5 (shown in Fig. 3a). It varies from 9 to13 Å^2 in the pressure range of 1 to 4 mN/m. On the other hand, the excess Gibb's free energy, ΔG_{exc}, for the mixed monolayer at certain surface pressures is obtained by integrating the excess area over surface pressure [38]. It is given by

$$\Delta G_{exc} = N_a \int_{\pi^*}^{\pi} A_{exc} d\pi \tag{2}$$

where $\pi*$ is the surface pressure where the two components of the mixed monolayer act ideally (normally taken as zero), π is the upper limit of pressure at which the integral is calculated and N_a is the Avogadro number. Now three situations may arise: (i) ΔG_{exc} = 0, components of monolayer are mixed ideally or totally immiscible, (ii) $\Delta G_{exc} > 0$, their interactions between components are repulsive, (iii) $\Delta G_{exc} < 0$, interactions are attractive. Fig. 3b shows ΔG_{exc} as a function of X_{CHS} at three selected surface pressures (π = 1, 2 and 4 mN/m). The positive departure from $\Delta G_{exc} = 0$ value (i.e. dash-dot line) in the entire range of mole fraction of CHS demonstrates the presence of repulsive interaction between components. The departure is found to be maximum at X_{CHS} = 0.5, which implies that the repulsive interaction is dominant at this mole fraction.

To elucidate the influence of CHS molecules on the viscoelastic properties of SA monolayer, the compressional modulus C_s^{-1} of the mixed films was calculated from π-A isotherms. C_s^{-1}, which is the reciprocal of the monolayer compressibility (C_s), is defined as

$$C_s^{-1} = -A\frac{d\pi}{dA}. \tag{3}$$

It can also be called as the equilibrium in-plane elasticity. The elasticity of the hybrid monolayers, as depicted in Fig. 4, was affected by addition of CHS. The pure SA monolayer exhibits higher values of C_s^{-1} with compression (i.e. low area per molecule). A drastic reduction of elasticity with the inclusion of CHS is encountered. Fig. 4b illustrates that the elasticity attains its maximum value around the pressure range 25–45 mN/m for mixed monolayer and 30–50 mN/m for pure SA. At low surface pressures (<20 mN/m), when the area per molecule is large, the elasticity is found comparable for pure and mixed monolayers. At high pressure (>20 mN/m), when the monolayers are close packed, their elasticity differ from each other significantly. Furthermore, in order to examine the stability of mixed monolayer, we performed hysteresis (i.e. compression-decompression cycle) measurement (see Supporting Information S1). No significant hysteresis is observed for all three mixtures. It implies that the monolayers are stable and reversible. Nath et al. [39] reported a drastic hysteresis for CHS-arachidic acid mixture when the concentration of CHS is >0.125 M. Below this concentration no hysteresis was observed. In the present study, we used 50 mM concentration of CHS, which is still much lower than the reported one. Hence our results are in consistent with Nath et al.

3.1.3. Temperature dependent isotherm of mixed monolayer

Isotherms of CHS-SA mixed monolayer depicted in Fig. 5a are recorded with varying temperature from 22 °C to 8 °C keeping the other experimental parameters same. The diminution of temperature of subphase water causes an expansion of area per molecule at air-water interface. The extrapolated area (A_{ex}) is increased from 22 to 26 Å^2/molecule. The expansion is accompanied by a substantial reduction of π_c and $\pi_{L\text{-}S}$ from 60 to 50 mN/m and 24 to 20 mN/m, respectively. Nevertheless, surface tension or surface pressure itself depends on temperature. Surface pressure is known

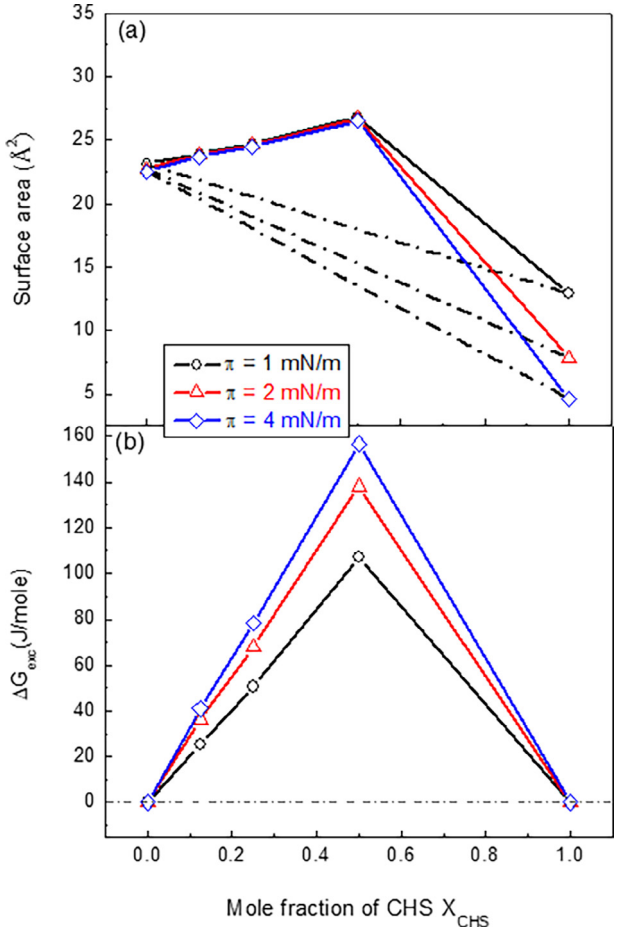

Fig. 3. (a) Evolution of the experimentally determined area per molecule A_{12} (continuous line plus symbol) and the calculated ideal area per molecule A_{id} (dashed-dot line) with mole fraction of CHS in CHS-SA mixed monolayers at three different pressures. The difference between A_{12} and A_{id} is assigned as excess area A_{exc}. (b) The variation of excess Gibb's free energy, ΔG_{exc} with mole fraction (X_{CHS}) of CHS in SA, computed at different surface pressures.

to decrease with temperature because cohesive forces decrease with an increase of molecular thermal motion. For the reference, we also investigate the evolution of isotherm of pure SA monolayer as a function of temperature (shown in the inset of Fig. 5a). A little decrease in pressure, which is the basic characteristic of surface tension, is evident. Therefore, the drastic decrement in surface pressure of mixed monolayer with temperature must be attributed to presence of CHS in CHS-SA mixed monolayer. In addition, slope of the isotherms, which is a measure of elasticity, progressively decreases with temperature. The elasticity is found to drop substantially from 2032 to 897 mN/m, indicating the further inclusion of soft CHS molecules into binary monolayer suspended on water surface. Probably the solubility of CHS decreases with the reduction of temperature. Similar behavior was encountered for Vitamin C by Neto et al. [40] and Shalmashi et al. [41] They correlated the mole fraction solubility N of Vitamin C as a function of temperature (T) as follows

$$\ln N = A + B(T/K), \tag{4}$$

where A and B are the parameters depend on the nature of the solvent. Therefore, Eq. (4) indicates that decrease in temperature hinders the solubility. Similarly we can assume that the decay in temperature compelled CHS to be more populated at the air-water interface. To the best of our knowledge, no such survey on CHS exists in the literature. The presence of soft component, namely CHS, makes the SA monolayer sheet more fluidic or flexible at air-water interface. This flexibility assists collapse to take place at lower pressure.

3.2. Structure of Langmuir-Blodgett films

LB films of hybrid monolayer were deposited on hydrophilic native oxide covered silicon (labeled as SiO_x-Si) at two surface pressures, such as 30 and 15 mN/m. The reason behind this selection of pressure was that these pressures correspond two different phases i.e. solid and liquid (as shown in Fig. 2) respectively, which might give rise to different structures. Owing to the polar nature of native oxide [42], deposition was made in upstroke (one) sequence starting from the bottom of water subphase.

3.2.1. X-ray reflectivity and atomic force microscopy study

To probe the structure of LB films of CHS-SA hybrid monolayer, we performed XRR measurements. As the XRR technique provides EDP along depth, it is possible to find out the out-of-plane structure of LB films. By knowing this structure one can endorse the presence of CHS at the interface and verify the possibility of relocating the CHS together with SA on SiO_x-Si (1 0 0).

XRR data and analyzed curves for three different mixed layers are shown in Fig. 6. Bi-layer feature is evident in XRR curves especially for 1:1 hybrid film. However, to get the quantitative

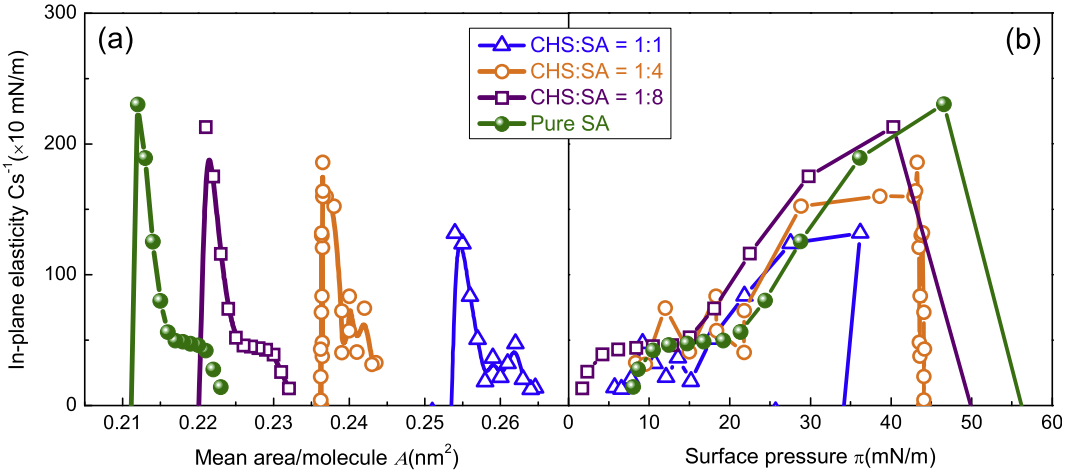

Fig. 4. In-plane elasticity C_s^{-1} of CHS-SA hybrid films as a function of (a) mean area/molecule and (b) surface pressure with variation in CHS mole fraction.

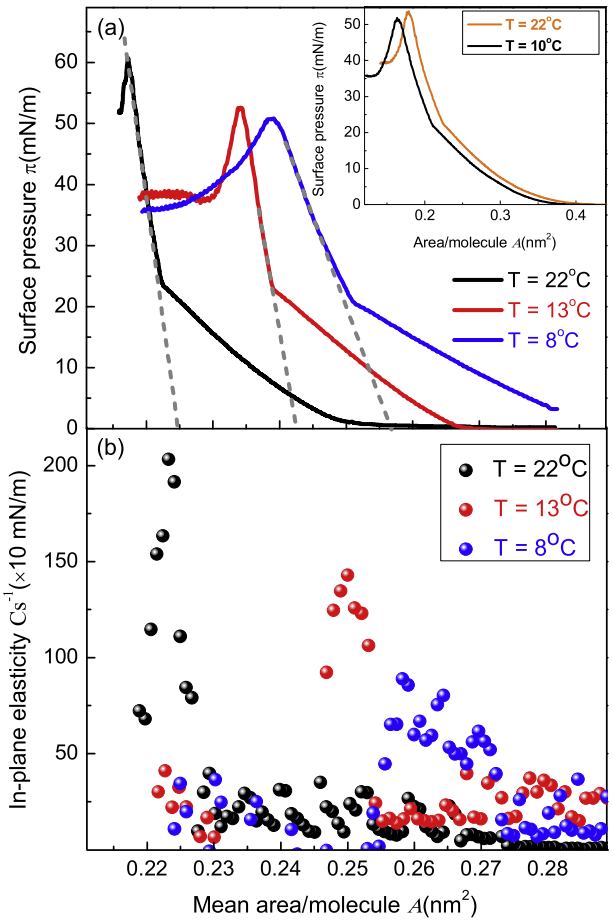

Fig. 5. (a) Isotherm study of CHS-SA (1:8) mixture with variation in temperature. Inset shows isotherm of stearic acid at two different temperatures. Extrapolated area (A_{ex}) is shown by dashed lines. (b) Effect of temperature on in-plane elasticity of CHS-SA mixed monolayer.

information about the structure and structural differences all the XRR data were fitted by considering a realistic model structure and corresponding EDPs are given in their insets.

For the fitting each films are divided into different box or layers as shown in Table 1. Each box or layer carries constant density and roughness is incorporated at each interfaces. There are three fitting parameters, such as thickness, density and roughness of each box or layer. EDP apparently suggests that a bilayer of total thickness ≈ 6.5 nm is formed when the film deposited at π = 30 mN/m. To get this bilayer-like feature the films are sliced into three layers. *Bottom* layer (corresponds to L1) is much denser than the *middle* layer (corresponds to L2) and *top* layer (corresponds to L3). From the density profile it can be observed that electron density of *bottom* layer and *top* layer varies from 0.347 to 0.366 e/Å^{-3} and 0.081 to 0.113 e/Å^{-3} respectively when the mixed ratio varies from 1:8 to 1:1. These densities are slightly different from the densities presented in the table. Because tabulated densities are the fitting parameters whereas the densities obtained from EDP are the effective densities that are convoluted with roughness. However, normally one cannot expect a bi-layer-like structure from pure SA in one stroke (up) at π = 30 mN/m [43]. Hence in the present study, the formation of bi-layer can be attributed to the hybrid interaction between CHS and SA. Indirectly, it indicates the presence of CHS within the Langmuir monolayer and LB films. On the other hand a monolayer of thickness ≈ 2.6 nm is formed for film deposited at 15 mN/m. Notably for the sake of better fitting of XRR data (as shown in Fig. 6b), these films are dissected into two layers (L1 and L2, given in Table 1) although they do not appear as bi-layer in EDP rather they constitute monolayer. The low density third layer is disappeared in the films which were deposited at low surface pressure. Monolayer characteristics is directly encountered in the surface topography images (shown in Fig. 7a–c) obtained from AFM, whereas a bi-layer nature is evident in the Fig. 7d–f. Heights obtained from AFM images are in well agreement with the thicknesses of the films measured by XRR. Furthermore, the coverage of the films on substrate are obtained from the bearing plot of AFM images using WSxM software. The coverages of films prepared at π = 15 mN/m from solutions 1:1, 1:4 and 1:8 are ≈57, 43 and 41%, respectively. Similarly their coverages obtained at π = 30 mN/m from solutions 1:1, 1:4 and 1:8 are ≈95, 97 and 98%. Unfortunately, it is not possible to estimate these coverages from EDP as the system is binary and we do not know what the relative percentage of molecules constituting the film is. Normally the density of a layer is deduced from EDP considering the bulk density of layer material as 100% [30, 31]. Here one assumption stating that

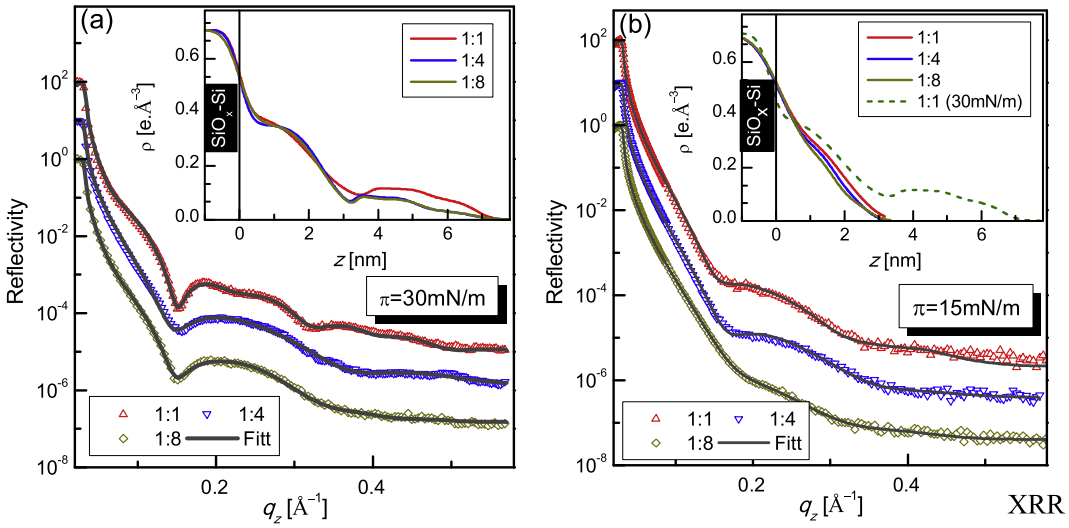

Fig. 6. XRR data (different symbols) and analyzed curves (solid line) of CHS-SA hybrid LB film on hydrophilized Si (1 0 0) substrate, deposited by one upstroke at two different surface pressures (a) π = 30 mN/m and (b) π = 15 mN/m (curves are shifted vertically for clarity). Inset: corresponding EDPs showing possible structures of LB films.

Table 1
Parameters, such as thickness (d), electron density (ρ) and surface interface roughness (σ) of different films obtained from X-ray reflectivity analysis (i.e. EDP) assuming a model structure. Each film prepared at π = 15 mN/m divided into two constituent layers (L1 and L2) whereas films deposited at π = 30 mN/m divided into three constituent layers (L1, L2 and L3). In every fitting a 20 Å native oxide layer is added on top of Si substrate.

Deposition pressure (mN/m)	Films divided into layers		Density ρ(e/Å^3)	Thickness (Å)	Roughness σ(Å)
π = 15	1:1	L1	0.286	16.1	4.3
		L2	0.149	8.4	5.1
	1:4	L1	0.268	16.2	3.9
		L2	0.099	8.5	3.7
	1:8	L1	0.230	15.3	3.7
		L2	0.074	9.7	3.6
π = 30	1:1	L1	0.367	21.3	9.0
		L2	0.030	16.3	2.8
		L3	0.096	26.8	7.6
	1:4	L1	0.347	23.3	6.3
		L2	0.018	10.8	3.6
		L3	0.057	18.8	7.7
	1:8	L1	0.347	22.8	6.7
		L2	0.022	11.9	3.3
		L3	0.054	25.3	7.5

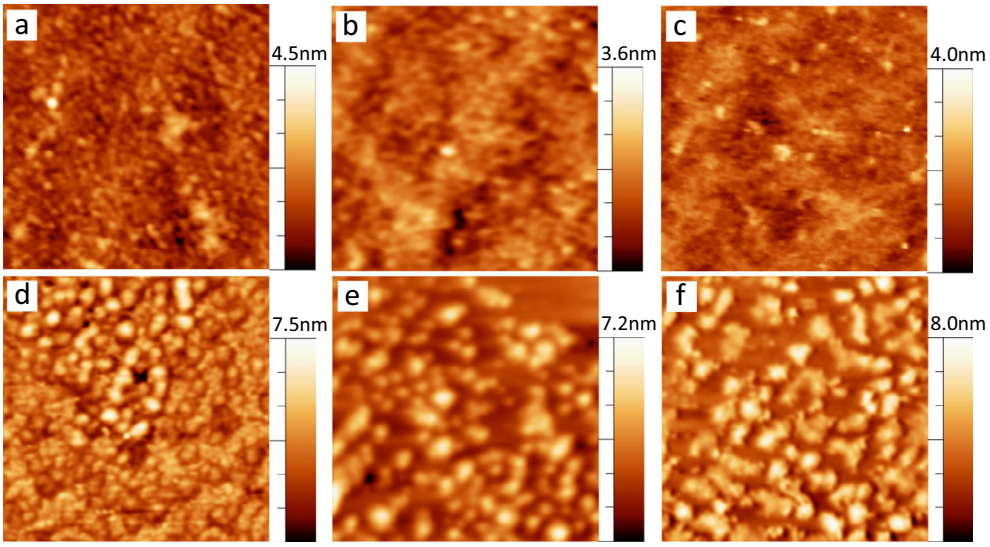

Fig. 7. AFM images (Scan area = 500×500 nm^2) of CHS-SA hybrid LB films on hydrophilized Si (1 0 0) substrate deposited by one upstroke. Images a, b and c are obtained from hybrid films 1:1, 1:4 and 1:8 deposited at π = 15 mN/m whereas d, e and f are obtained from the same mixture transferred at high pressure π = 30 mN/m. Cray scales are given adjacent to the images.

the compactness in bulk and ultrathin films remains the same is made.

3.2.2. Fourier transform infrared spectroscopy study

FTIR measurements were carried out of pure CHS, pure SA and CHS-SA mixed films using Jasco FT/IR-6300 in the wavelength range of 600 cm^{-1}to 3800 cm^{-1}. The assigned characteristic FTIR adsorption bands derived from Fig. 8 are summarized in Table 2. The main bands appearing in the spectrum of pure CHS are due to stretching vibrations of O—H group in the range from 3000 cm^{-1} to 3700 cm^{-1}, which are overlapped with the stretching vibration of N—H; C—H bond in —CH_2 (at 2920 cm^{-1}) and —CH_3 (at 2878 cm^{-1}) groups [44, 45]. Bending vibrations of methylene and methyl groups are also visible at 1337 cm^{-1} and 1427 cm^{-1}, respectively. Adsorption at 1648 cm^{-1} is related to the vibrations of carbonyl bonds (C═O) of the secondary amide group whereas the adsorption at 1571 cm^{-1} can be attributed to the vibrations of protonated amine group. The dip located at 1153 cm^{-1} is related to asymmetric vibrations of CO in the oxygen bridge resulting from deacetylation of CHS. The dips at 1070 cm^{-1} and 1029 cm^{-1} are assigned to the vibrations of CO in the ring COH, COC and CH_2OH. The small dip at 856 cm^{-1}corresponds to wagging of the saccharide structure of CHS. Similarly for pure SA the main bands are obtained at 2921 cm^{-1} and 2851 cm^{-1} due to asymmetric —CH_3 and symmetric —CH_2 groups, respectively. The peak at about 1705 cm^{-1} is attributed to C═O stretching vibrations. A band appears near 1465 cm^{-1} is assigned to scissor band of CH_2. At lower wavenumbers, two bands appear at 934 and 721 cm^{-1} due to bending mode of hydrogen bond (OH—H) and stretching mode of C═O group, respectively. Compared to the IR spectrum of pure CHS and SA, the CHS-SA spectrum showed some changes in the band nature and intensity but their position remains unchanged (e.g. 2921, 2852, 1706, 1463, 934 and 721 cm^{-1}) to that of pure SA [44]. For the CHS-SA hybrid film some additional bands at 1568 and 1153 cm^{-1} corresponding to the characteristics of CHS are observed. Due to contribution of pure CHS band at 1648 cm^{-1} the 1706 cm^{-1} band of CHS-SA spectrum becomes broadened. Notably their intensity is very small due to the small quantity of CHS present in CHS-SA hybrid LB film. Additionally a broad hump around 3434 cm^{-1} similar to pure CHS is encountered. All these

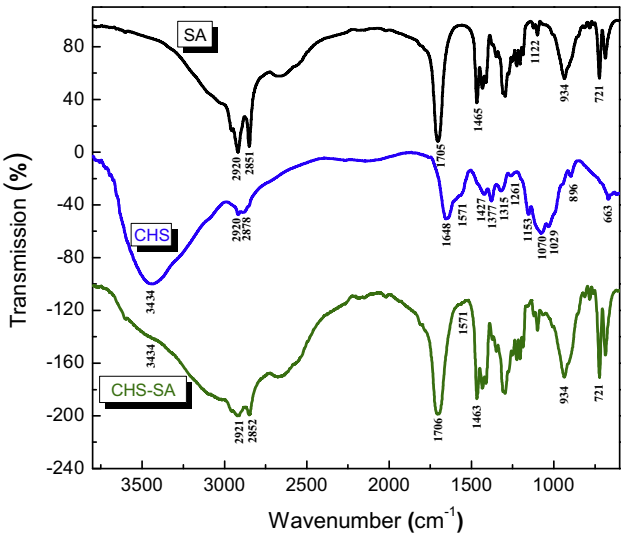

Fig. 8. Normalized FTIR spectra for pure CHS, pure SA and hybrid CHS-SA (1:8) films. Curves are shifted vertically for clarity.

Table 2
Assignment of FTIR spectra of pure SA, pure CHS and their hybrid films derived from Fig. 8.

Sample	IR Band (cm^{-1})	Description*
CHS	3750–3000	ν(O—H) overlapped with ν_s(N—H)
	2920	ν_{as}(C—H)
	2878	ν_s(C—H)
	1648	ν(—C=O) secondary amide
	1571	ν(—C=O) protonated amide
	1427,1377	δ(C—H)
	1315	ν_s(—CH_3) tertiary amide
	1261	ν_s(C—O—H)
	1153,1070,1029	ν_{as}(C—O—C) and ν_s(C—O—C)
	856	ω(C—H)
SA	2921	ν_{as}(C—H) CH_3
	2851	ν_s(C—H) CH_2
	1705	ν(—C=O) secondary amide
	1465	CH_2 scissoring
	1122	ν(—C—C)
	934	Bending vibration of H bond (OH—H)
	721	ν(C = O)
CHS-SA	2921	ν_{as}(C—H) CH_3
	2852	ν_s(C—H) CH_2
	1706	ν(—C=O) secondary amide
	1571	ν(—C=O) protonated amide
	1463	CH_2 scissoring
	934	Bending vibration of H bond (OH—H)
	721	ν(C=O)

* ν = stretching vibration; ν_s = symmetric stretching vibration; ν_{as} = asymmetric stretching vibration; ω = wagging.

results constitute the fact that CHS is present within the hybrid LB films. In comparison to pure SA, no appreciable shift in band position of common bands is detected in CHS-SA hybrid spectrum. This kind of shift one can expect for chemically grafted CHS with SA [45].

3.3. Model structure of CHS-SA hybrid layer and underlying mechanism

Based on the results obtained in the present work, we propose a model depicted in Fig. 9, which illustrates that pure CHS has negligible surface activity (Fig. 9a). This conclusion is drawn from the isotherm characteristics of pure CHS shown in Fig. 1. As the CHS has negligible surface activity it does not affect the surface pressure appreciably. However after mixing with SA, CHS exhibits drastic surface activity which is manifested in the isotherm characteristics (see Fig. 1 and Fig. 2). This is due to the fact that SA has great surface activity which force the hybrid mixture to show surface activity. Isotherm of CHS-SA suggests that, in presence of CHS molecules, the Langmuir monolayer of saturated fatty acid i.e. SA is reoriented and gets squeezed, whereas for unsaturated fatty acid the monolayer gets slackened [21]. In the condensed phase, SA resides on the top of water surface taking a cylindrical pillar-like shape with the hydrophilic head group attached with water and hydrophobic tail orienting towards upper direction in a systematical way. When CHS is added, it interacts with CHS by means of attractive force. Some of the CHS gets in between SA molecule pillars escalating the area of Langmuir monolayer. The possible interactions between CHS and SA molecules are: (1) The Carboxylic group (—COO^-), makes a complex with —NH_3^+ group by electrostatic interaction. (2) At lower pressure, CHS molecules interact with SA by hydrophobic interaction and this is how they penetrate into SA monolayer. But at higher pressure this mechanism is no longer valid as CHS is forced out from SA monolayer and resides in the subphase. At higher pressure, CHS probably interacts with SA polar heads by hydrogen bonding with addition to electrostatic interaction. Notably CHS can stick on fatty acid monolayers mainly by Coulombic interactions. Nonetheless, no shift in the IR band position for pure SA and CHS-SA films is encountered (see Fig. 8), rather band intensity modifies and some additional bands corresponding to CHS appear. However, a systematic increase in the area/molecule and decrease in elasticity with the progressive increment of soft component CHS suggest an appreciable surface activity in the mixed layer at air-water interface.

At low surface pressure (say π = 15 mN/m), when the area per molecule is large, the CHS chains partially infiltrate through SA molecular sheet at air-water interface (see Fig. 9b) and reside in the vicinity of hydrocarbon chains of SA by means of hydrophobic interactions [22]. Therefore, at low surface compactness both hydrophobic and electrostatic interactions are present. Due to these interactions, the shifts of surface pressure-area isotherms towards large molecular area are encountered. At high surface pressure (say π = 30 mN/m), when mean area per molecule is small, high population density may favor expelling of CHS molecules from the surface. Notably CHS is not expelled to the bulk water rather it forms a subsurface interacting with polar head of SA molecules through hydrogen bonding and electrostatic interactions. Here hydrophobic interactions might be abandoned because monolayer compression causes CHS to be located at the subsurface. Accordingly when we transferred onto solid substrate a bilayer stacking is observed (see Fig. 6a and 7d–f) at high pressure. In contrast a monolayer stacking is observed at low surface pressure (see Fig. 6b and 7a–c). These two conclusions are made based on the XRR and AFM analysis. The presence of CHS within the mixed films is confirmed from FTIR spectra (shown in Fig. 8). Furthermore no appreciable material is deposited in case of pure CHS as concluded from the transfer ratio (nearly zero) and XRR analysis (not shown here). These results confirm the molecular picture depicted in Fig. 9. Falling down of temperature allows CHS to reach at air-water interface from subsurface by reducing the solubility in water. Likewise the solubility of Vitamin C was found to be reduced with temperature [40, 41]. Accordingly the number of molecules at the air-water interface alters, causing a modification in area per molecule in the floating monolayer. Eventually, the role of CHS on SA monolayers at different pressures can have a resemblance with cell membranes. D. Marsh [46] reported that for separating the molecules by membrane the applicable parameter is the compressional modulus or in-plane elasticity rather than the lateral

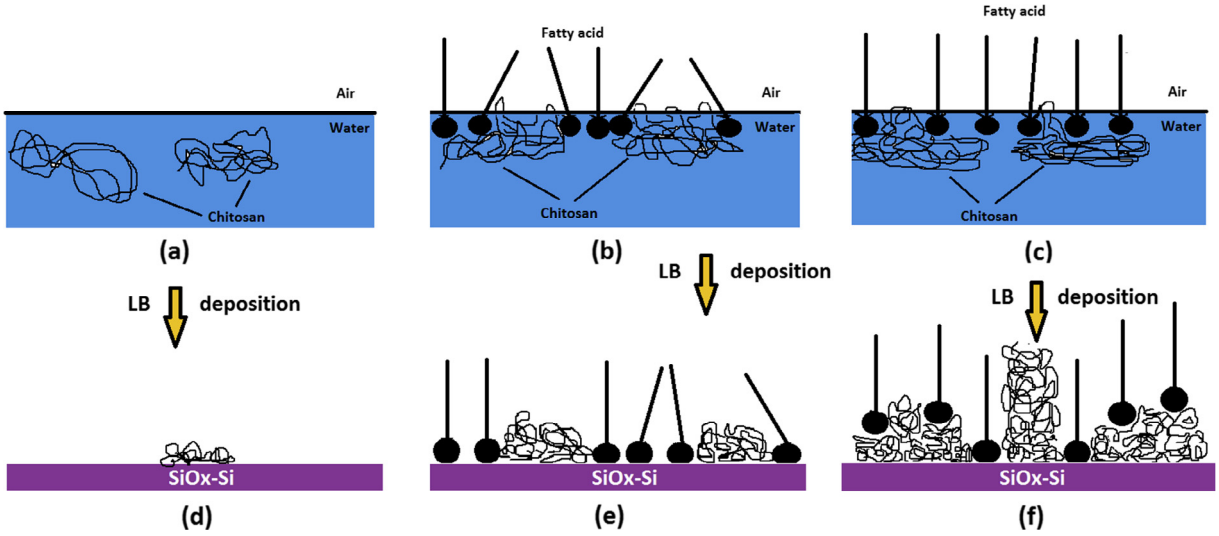

Fig. 9. Schematic diagram of (a) pure chitosan in water subphase and interaction with stearic acid at two different pressures (b) π = 15 mN/m and (c) π = 30 mN/m. (d), (e) and (f) corresponding LB films on SiO_x-Si substrate deposited in one upstroke sequence.

pressure difference. Many protein macromolecules reduce the elasticity of cell membrane after attachment. The work presented here demonstrates identical situations.

4. Conclusions

On the basis of the present study and previously reported literatures [21, 25], we have demonstrated that chitosan alone does not form self-supporting film at air-water interface, whereas chitosan mixed with stearic acid does. Chitosan insertion causes an expansion of chitosan-fatty acid hybrid monolayers and reduces the elasticity and make the film heterogeneous. Chitosan provokes local disruption of the fatty acid monolayer involving electrostatic, dipolar and hydrophobic interactions. The results could be rationalized in terms of a model in which at low surface pressure chitosan is situated at interface, interacting with stearic acid molecules via electrostatic and hydrophobic interactions whereas at high pressure chitosan mainly located at subsurface beneath stearic acid molecules. In the latter case the interaction is predominantly electrostatic yielding very small contribution to the surface pressure. Studies till date report the structure and mechanical properties of such hybrid monolayers only at room temperature [21–26]. Present study extends these properties towards low temperatures (down to 8 °C) along with thermodynamic stability. Reduction of temperature of subphase water allows more number of chitosan molecules to reach surface. Additionally, we have demonstrated that the chitosan could be transferred easily onto solid supports employing LB technique by mixing with fatty acid in subphase. The presence of chitosan within transferred films is confirmed from FTIR analysis. Their detailed structure extracted from XRR (out-of-plane) and AFM (in-plane) is found strongly dependent on chitosan mole fraction and deposition pressure. Previous studies reported their structure or conformation either based on the band position in FTIR spectrum [44], nanogravimetry measurements [23] or based on theoretical simulation [25] open up intricate possibilities of structure preventing any accurate modeling, while the present study is founded on two complementary surface sensitive (precision ~ few angstrom) techniques like XRR and AFM, which minimizes the uncertainty in modeling. By knowing the structure of solid supported films at various conditions, one can develop the organization or conformation of the pre-deposited films at air-water interface. This might lead to different model structures, which may have implications in the biological applications of chitosan in drug delivery and in biosensing devices.

Acknowledgements

J.K.B. thankfully acknowledged to Department of Science and Technology (DST), Government of India, for providing research grant through INSPIRE Faculty Award (IFA13-PH-79). The financial support received from the DST and ICTP under the India-Elettra access program to carry out XRR experiments at MCX beamline of Elettra is thankfully acknowledged.

Appendix A. Supplementary material

Supplementary data associated with this article can be found, in the online version, at https://doi.org/10.1016/j.jcis.2017.12.037.

References

[1] P. Calvo, C. Remunan-Lopez, J.L. VilaJato, M.J. Alonso, Development of positively charged colloidal drug carriers: Chitosan-coated polyester nanocapsules and submicron-emulsions, Colloid Polym. Sci. 275 (1997) 46–53.
[2] Y. Ohya, T. Takei, T. Ouchi, Thermo-sensitive release rehavior of 5-fluorouracil from chitosan-gel microspheres coated with lipid multilayers, J. Bioact. Compat. Polym. 7 (1992) 242–256.
[3] E.I. Rabea, M.E. Badawy, C.V. Stevens, G. Smagghe, W. Steurbaut, Chitosan as antimicrobial agent: Applications and mode of action, Biomacromolecules 4 (6) (2003) 1457–1465.
[4] L. Sun, Y. Du, J. Yang, X. Shi, J. Li, X. Wang, J.F. Kennedy, Conversion of crystal structure of the chitin to facilitate preparation of a 6-carboxychitin with moisture absorption–retention abilities, Carbohydr. Polym. 66 (2006) 168–175.
[5] C. Augustin, C. Collombel, O. Damour, Use of dermal equivalent and skin equivalent models for identifying phototoxic compounds in vitro, Photodermatol. Photoimmunol. Photomed. 13 (1997) 27–36.
[6] I. Agerkvist, Mechanisms of flocculation with chitosan in Escherichia coli disintegrates: effects of urea and chitosan characteristics, Colloids Surfaces 69 (1992) 173–187.
[7] P. Fäldt, B. Bergenstähl, P.M. Claesson, Stabilization by chitosan of soybean oil emulsions coated with phospholipid and glycocholic acid, Colloids Surf. A 71 (1993) 187–195.
[8] D.B. Allison, K.R. Fontaine, S. Heshka, J.L. Mentore, S.B. Heymsfield, Alternative treatments for weight loss: a critical review, Crit. Rev. Food Sci. Nutr. 41 (2001) 1–28.
[9] M.H. Pittler, E. Ernst, Complementary therapies for reducing body weight: a systematic review, Int. J. Obes. 29 (2005) 1030–1038.

[10] S. Magdassi, U. Bach, K.Y. Mumcuoglu, Formation of positively charged microcapsules based on chitosan-lecithin interactions, J. Microencapsulation 14 (2) (1997) 189–195.
[11] K. Sathirakul, Advances in Chitin Science, R.H. Chen, H.C. Chen (Eds.), Rita Adv.: Taiwan, 3 (1999), pp. 469–474.
[12] R.A.A. Muzzarelli, N. Frega, M. Miliani, C. Muzzarelli, M. Cartolari, Interactions of chitin, chitosan, N-lauryl chitosan and N-dimethylaminopropyl chitosan with olive oil, Carbohydr. Polym. 43 (2000) 263–268.
[13] N. Thotakura, M. Dadarwal, P. Kumar, G. Sharma, S.K. Guru, S. Bhushan, K. Raza, O.P. Katare, Chitosan-stearic acid based polymeric micelles for the effective delivery of tamoxifen: cytotoxic and pharmacokinetic evaluation, AAPS PharmSciTech 18 (2017) 759–768.
[14] H. Yokoi, S. Hayashi, T. Kinoshita, Polypeptide membranes at an interface, Prog. Polym. Sci. 28 (2003) 341–357.
[15] H. Brockman, Lipid monolayers: why use half a membrane to characterize protein-membrane interactions?, Curr Opin. Struct. Biol. 9 (1999) 438–443.
[16] M.C. Petty, Langmuir-Blodgett films, An Introduction, Cambridge University Press, New York, 1996.
[17] J. Desbrieres, Viscosity of semiflexible chitosan solutions: influence of concentration, temperature, and role of intermolecular interactions, Biomacromolecules 3 (2002) 342–349.
[18] H.-F. Guo, H.-L. Lin, T.L. Yu, Dilute solution properties of chitosan in propionic acid aqueous solutions, J. Macromol. Sci. Part APure Appl. Chem. 39 (2002) 837–852.
[19] E. Buhler, M. Rinaudo, Structural and dynamical properties of semirigid polyelectrolyte solutions: a light-scattering study, Macromolecules 33 (6) (2000) 2098–2106.
[20] R.G. Beri, J. Walker, E.T. Reese, J.E. Rollings, Characterization of chitosans via coupled size-exclusion chromatography and multiple-angle laser light-scattering technique, Carbohydr. Res. 238 (1993) 11–26.
[21] P. Wydro, B. Krajewska, K. Hac-Wydro, Chitosan as a lipid binder: a Langmuir monolayer study of chitosan-lipid interactions, Biomacromolecules 8 (2007) 2611–2617.
[22] F.J. Pavinatto, A. Pavinatto, L. Caseli, D.S.dos. Santos Jr, T.M. Nobre, M.E.D. Zaniquelli, O.N. Oliveira Jr., Interaction of chitosan with cell membrane models at the air-water interface, Biomacromolecules 8 (2007) 1633–1640.
[23] F.J. Pavinatto, L. Caseli, A. Pavinatto, D.S.dos. Santos Jr, T.M. Nobre, M.E.D. Zaniquelli, H.S. Silva, P.B. Miranda, O.N. Oliveira Jr, Probing chitosan and phospholipid interactions using Langmuir and Langmuir-Blodgett films as cell membrane models, Langmuir 23 (14) (2007) 7666–7671.
[24] N. Fang, V. Chan, Chitosan-induced restructuration of a mica-supported phospholipid bilayer: an atomic force microscopy study, Biomacromolecules 4 (2003) 1596–1604.
[25] H. Parra-Barraza, M.G. Burboa, M. Sánchez-Vázquez, J. Juárez, F.M. Goycoolea, M.A. Valdez, Chitosan-cholesterol and chitosan-stearic acid interactions at the air-water interface, Biomacromolecules 6 (2005) 2416–2426.
[26] G. Qun, W. Ajun, Effects of molecular weight, degree of acetylation and ionic strength on surface tension of chitosan in dilute solution, Carbohydr. Polym. 64 (2006) 29–36.
[27] J.K. Bal, T. Beuvier, A.B. Unni, E.A.C. Panduro, G. Vignaud, N. Delorme, M.S. Chebil, Y. Grohens, A. Gibaud, Stability of polymer ultrathin films (<7 nm) made by a top-down approach, ACS Nano 9 (2015) 8184–8193.
[28] L. Rebuffi, J.R. Plaisier, M. Abdellatief, A. Lausi, P. Scardi, MCX: A synchrotron radiation beamline for X-ray diffraction line profile analysis, Zeitschrift fur Anorg. und Allg. Chemie 640 (2014) 3100–3106.
[29] J. Daillant, A. Gibaud, X-ray and Neutron Reflectivity: Principles and Applications, Springer, Berlin, 1999.
[30] J.K. Bal, M. Mukherjee, N. Delorme, M.K. Sanyal, A. Gibaud, Concentration mediated structural transition of triblock copolymer ultrathin films, Langmuir 30 (2014) 5808–5816.
[31] J.K. Bal, T. Beuvier, M.S. Chebil, G. Vignaud, Y. Grohens, M.K. Sanyal, A. Gibaud, Relaxation of ultrathin polystyrene films hyperswollen in supercritical carbon dioxide, Macromolecules 47 (24) (2014) 8738–8747.
[32] J.K. Bal, S. Hazra, Interfacial role in room-temperature diffusion of Au into Si substrates, Phys. Rev. B 75 (20) (2007) 205411-1–6.
[33] I. Horcas, R. Fernández, J.M. Gómez-Rodríquez, J. Colchero, J. Gómez-Herrero, A.M. Baro, WSXM: a software for scanning probe microscopy and a tool for nanotechnology, Rev. Sci. Instrum 78 (1) (2007) 013705-1–8.
[34] R. Seoane, J. Min?ones, O. Conde, J. Min?ones Jr, M. Casas, E. Iribarnegaray, Thermodynamic and brewster angle microscopy studies of fatty acid/cholesterol mixtures at the air/water interface, J. Phys. Chem. B. 104 (2000) 7735–7744.
[35] M.A. Valdes-Covarrubias, R.D. Cadena-Nava, E. Vásquez-Martínez, D. Valdez-Pérez, J. Ruiz-García, J. Phys. Condens. Matter 16 (2004), 2097–2107.
[36] L. Gargallo, A. Leiva, M. Urzúa, L. Alegría, B. Miranda, D. Radić, Modification of the air-water interface by a chitosan adsorption process. Effect on an amphiphilic polymer monolayer, Polym. Int. 53 (2004) 1652–1657.
[37] G.L. Gaines Jr., Insoluble Monolayers at Liquid-Gas Interfaces, Wiley Interscience, New York, 1966.
[38] F.C. Goodrich, in: Proc. 2nd International Congress on Surface Activity, Butterworth, London, vol. I, M33, 1957.
[39] J. Nath, R.K. Nath, A. Chakraborty, S.A. Husain, Monolayer characteristics of chitosan assembled in Langmuir films mixed with arachidic acid, Surf. Rev. Lett 21 (4) (2014) 1450049-1–8.
[40] A.C.R. Neto, R.F. Pires, R.A. Malagoni, M.R. FrancoJr, Solubility of vitamin C in water, ethanol, propan-1-ol, water + ethanol, and water + propan-1-ol at (298.15 and 308.15) K, J. Chem. Eng. Data 55 (2010) 1718–1721.
[41] A. Shalmashi, A. Eliassi, Solubility of L-(+)-ascorbic acid in water, ethanol, methanol, propan-2-ol, acetone, acetonitrile, ethyl acetate, and tetrahydrofuran from (293 to 323) K, J. Chem. Eng. Data 53 (2008) 1332–1334.
[42] J.K. Bal, S. Kundu, S. Hazra, Hydrophobic to hydrophilic transition of HF-treated Si surface during Langmuir-Blodgett film deposition, Chem. Phys. Lett. 500 (2010) 90–95.
[43] J.K. Bal, S. Kundu, S. Hazra, Growth and stability of Langmuir-Blodgett films on OH-, H-, or Br-terminated Si(001), Phys. Rev. B 81 (2010). 045404-1-8.
[44] K. Barbara, W. Paweł, J. Agnieszka, Probing the modes of antibacterial activity of chitosan. Effects of pH and molecular weight on chitosan interactions with membrane lipids in Langmuir films, Biomacromolecules 12 (2011) 4144–4152.
[45] E. Moazeni, K. Gilani, A.R. Najafabadi, M.R. Rouini, N. Mohajel, M. Amini, M.A. Barghi, Preparation and evaluation of inhalable itraconazole chitosan based polymeric micelles, DARU J. Pharm. Sci. 20 (2012) 85.
[46] D. Marsh, Lateral pressure in membranes, Biochim. Biophys. Acta 1286 (1996) 183–223.